Available online at www.sciencedirect.com
ScienceDirect
Journal of Geodynamics 43 (2007) 450–464
JOURNAL OF GEODYNAMICS
http://www.elsevier.com/locate/jog

Softening of the subcontinental lithospheric mantle by asthenosphere melts and the continental extension/oceanic spreading transition☆

G. Ranalli [a,*], G.B. Piccardo [b], P. Corona-Chávez [c]

[a] Department of Earth Sciences and Ottawa-Carleton Geoscience Centre, Carleton University, Ottawa K1S 5B6, Canada
[b] Dipartimento per lo Studio del Territorio e delle sue Risorse (DIPTERIS), Università di Genova, 16132 Genova, Italy
[c] Instituto de Investigaciones Metalúrgicas, Universidad Michoacana de San Nicolás de Hidalgo, Morelia, Michoacán, Mexico

Received 6 February 2006; received in revised form 13 October 2006; accepted 18 October 2006

Abstract

The majority of ophiolitic peridotites in the Alpine–Apennine system show evidence of extensive interaction between subcontinental lithospheric mantle and fractional melts of asthenospheric origin. This interaction led to petrological, structural, and geochemical changes in the lithospheric mantle, and was accompanied by a temperature increase to near-asthenospheric values, resulting in the thermomechanical erosion of the lithosphere. We term the parts of mantle lithosphere thus affected the asthenospherized lithospheric mantle or ALM.

The thermal and rheological consequences of thermomechanical erosion are explored by modelling the temperature and rheological properties of the thinned lithosphere as a function of thickness of ALM and time since asthenospherization (i.e., since the beginning of thermal relaxation). Results are given both in terms of rheological profiles (strength envelopes) and total lithospheric strength (TLS) for different lower crustal rheologies. The TLS decreases as a consequence of thermomechanical erosion. This decrease is a non-linear function of the thickness of the ALM. While practically negligible if less than 50% of lithospheric mantle is affected, it becomes significant (up to almost one order of magnitude) if thermomechanical erosion approaches the Moho. The maximum decrease in TLS is achieved within a short time span (∼1–2 Ma) after the end of the heating episode.

As a working hypothesis, we propose that thermomechanical erosion of the lithospheric mantle, related to lithosphere/asthenospheric melts interaction, can be an important factor in a geologically rapid decrease in TLS. This softening could lead to whole lithospheric failure and consequently to a transition from continental extension to oceanic spreading.

Keywords: Continental extension; Oceanic spreading; Thermomechanical erosion of the lithosphere; Rheology; Total lithospheric strength

1. Introduction and geological background

Ophiolitic peridotites exposed along the Western Alps–Northern Apennine orogenic belt represent mantle sections of the oceanic lithosphere of the Ligurian Tethys, which separated the European and African (Adria) plates during Late Jurassic-Cretaceous times (Fig. 1). Petrologic, geochemical and isotopic evidence shows that, in many areas of the Alps

☆ Paper presented at the Peridotite Workshop 2005, held in Lanzo, September 27–30, 2005, organized by Alessandra Montanini and Giovanni B. Piccardo, and sponsored by the Italian Working Group on Mediterranean Ophiolites.

* Corresponding author. Tel.: +1 613 5204397; fax: +1 613 5202569.
E-mail address: granalli@earthsci.carleton.ca (G. Ranalli).

0264-3707/$ – see front matter © 2006 Elsevier Ltd. All rights reserved.
doi:10.1016/j.jog.2006.10.005

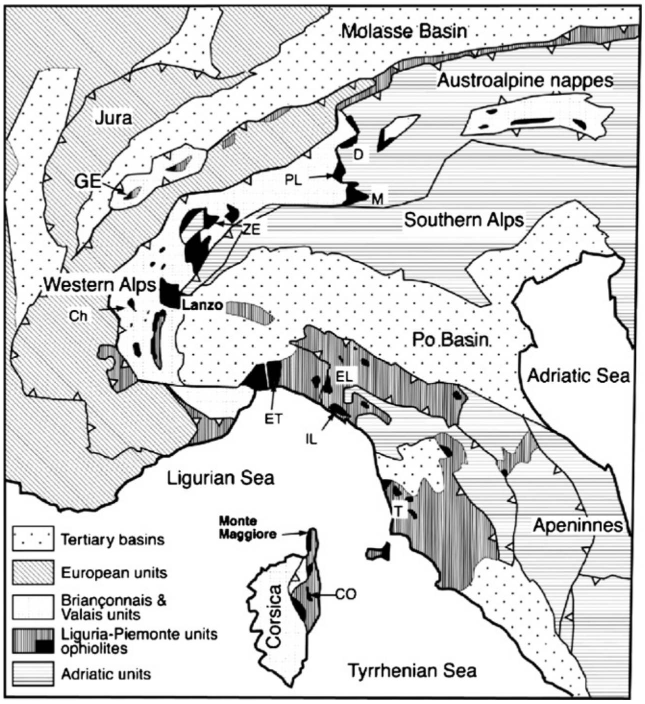

Fig. 1. Generalized tectonic overview of the Alpine–Northern Apennine ophiolites (redrawn and modified after Piccardo et al., 2004a). Keys: D, Totalp peridotite; PL, Platta ophiolite; M, Malenco peridotite; ZE, Saas Zermatt ophiolite; Ch, Chenaillet ophiolite; ET, Erro-Tobbio peridotite; EL, External Ligurides ophiolite; IL, Internal Ligurides ophiolite; T, Tuscan ophiolite; CO, Corsica ophiolite; GE, Gets ophiolite.

and Apennines, ophiolitic peridotites represent former subcontinental mantle (Piccardo, 1976; Piccardo et al., 1990; Trommsdorff et al., 1993; Rampone et al., 1995, 1998; Muntener and Hermann, 1996; Rampone and Piccardo, 2000). The opening of the Ligurian Tethys was kinematically related to Triassic to Early Jurassic rifting and Late Jurassic spreading in the central Atlantic (Dewey et al., 1973; Lemoine et al., 1987), and was driven by the passive extension of the Europe-Adria lithosphere. Rifting was recorded in the lithospheric mantle by the development of extensional shear zones (Drury et al., 1990; Vissers et al., 1991; Strating et al., 1993), leading to the gradual upwelling of sectors of spinel-facies lithospheric mantle, and by incipient recrystallization under decompression to plagioclase-facies conditions (Piccardo, 1976; Rampone et al., 1993, 1995; Müntener et al., 2000; Piccardo et al., 2004a,b).

After exhumation to shallow crustal levels, the lithospheric peridotites were intruded by MORB melts, forming km-scale gabbroic cumulate bodies and m-scale gabbroic and basaltic dykes, and were exposed on the seafloor, where they were discontinuously covered by MORB lava flows and Upper Jurassic radiolarian cherts (Piccardo et al., 2004a,b, and references therein). The occurrence of primary melts with typical MORB affinity intruding the extending mantle lithosphere indicates that lithosphere extension and thinning was accompanied by near-adiabatic upwelling and decompression partial melting of the underlying asthenosphere.

The atypical association of MORB magmatism and fertile subcontinental mantle has led to the suggestion that the Alpine–Apennine ophiolites are different from oceanic lithosphere formed at mature mid-ocean ridges (Decandia and Elter, 1972; Piccardo, 1976), but were formed during the early stages of opening of the Ligurian Tethys, by extension and thinning of continental lithosphere and final breakup of the crust that resulted in the exposure of subcontinental mantle at the seafloor (Piccardo, 1977; Beccaluva and Piccardo, 1978; Lemoine et al., 1987).

Recent field, petrological and geochemical studies on these ophiolitic peridotites have shown that, before intrusion and extrusion of aggregate MORB melts, pristine spinel-facies lithospheric peridotites were diffusely transformed to granular, depleted-enriched peridotitic rock types, which show petrographic-microstructural and geochemical characteristics indicative of melt–rock interaction processes. The evidence suggests that melt fractions from the asthenosphere migrated upwards by diffuse porous flow through, and reacted with, the overlying extending lithosphere, causing significant structural and compositional modifications (Müntener and Piccardo, 2003; Piccardo, 2003; Piccardo et al., 2004a,b, 2005, in press, 2007, and references therein).

Lithospheric peridotites were initially percolated via diffuse porous flow by pyroxene(-silica)-undersaturated fractional melt increments at spinel-facies conditions ($P > 1$ GPa) and temperature conditions close to the dry peridotite solidus. Reactively ascending hot liquids dissolved pyroxene and precipitated olivine, transforming the lithospheric mantle protoliths to depleted reactive peridotites. At shallower levels, under plagioclase-facies conditions, both lithospheric and reactive spinel peridotites were percolated and impregnated by orthopyroxene(-silica)-saturated fractional melt increments. Liquids ascending by reactive porous flow partially dissolved olivine and precipitated orthopyroxene (±clinopyroxene) and plagioclase in the form of microgranular, plagioclase-rich gabbroic aggregates. Accordingly, previous spinel peridotites were transformed to refertilized, impregnated plagioclase peridotites, enriched in basaltic components, at temperature conditions close to the liquidus temperature of the migrating melts.

The distribution and abundance of melt-modified spinel and plagioclase peridotites within the ophiolitic peridotites of the Ligurian Tethys indicate that substantial volumes of pristine lithospheric mantle underwent these melt-related processes along the axial zone of the future basin (Piccardo et al., 2004a,b, in press, 2007).

The evidence suggests that temperature conditions of percolating melt and host peridotite were close to the liquidus of anhydrous basaltic melts (i.e., $T \sim 1250$–$1300\,°C$) at depths compatible with spinel and plagioclase facies conditions (Piccardo et al., 2005; Müntener et al., 2005) This conclusion is supported by geothermometric data obtained from trace element distribution between coexisting mantle minerals in the percolated peridotites (method of Seitz et al., 1999) which show that (i) reactive spinel peridotites equilibrated at $T = 1200$–$1300\,°C$ at spinel facies conditions and (ii) plagioclase peridotites equilibrated at $T = 1150$–$1270\,°C$ at plagioclase facies conditions. In contrast, other ophiolitic peridotites from the Ligurian Tethys, including spinel peridotites from the same massifs, which escaped melt impregnation, usually record equilibration temperatures of about 1000 °C at spinel facies conditions (cf. Piccardo et al., 2004a).

It can therefore be deduced that melt percolation processes were active from the top of the partially molten asthenosphere to shallow levels. Consequently, temperature in the whole percolated and impregnated lithosphere must have been higher than or close to the liquidus of anhydrous basaltic melts, i.e., significantly higher than typical lithospheric temperatures.

Thus, upwelling hot asthenosphere and diffuse porous flow of asthenospheric melts was accompanied by a temperature increase in the affected lithospheric mantle that brought it above the liquidus of percolating melts and close to the dry peridotite solidus, i.e., practically to asthenospheric temperatures (Piccardo, 2003). From the thermal viewpoint, therefore, the lithospheric mantle was asthenospherized, i.e., it acquired asthenospheric characteristics (Müntener et al., 2005). We refer to it as “asthenospherized lithospheric mantle” (ALM) to emphasize that it is the result of the thermomechanical erosion of the lithosphere related to the percolation of asthenospheric melts.

In this paper, we model the thermal and rheological consequences of an episode of heating accompanying the diffuse percolation and impregnation of asthenospheric melts in an overlying extending lithosphere. We estimate the magnitude of the relative decrease in total lithospheric strength caused by thermomechanical erosion, as a function of both thickness of ALM and time since asthenospherization. We hypothesize that this decrease in total strength could be a factor favouring (or controlling) the transition from continental rifting (which does not involve the complete failure of the lithosphere) to oceanic spreading, i.e., a factor in determining whether passive continental extension can evolve into plate separation and the formation of a new ocean.

2. Model

2.1. Preliminary considerations: percolation velocity and ALM temperature

The starting point of the model of thermomechanical erosion of the lithosphere is based on two sets of observations, namely: (i) diffuse porous flow from the asthenosphere was able to affect large volumes of lithospheric mantle and (ii) the temperature of the affected volumes increased significantly at the same time. We do not discuss here theoretical models of melt percolation in a solid matrix (cf. e.g., McKenzie, 1985, 1989; Vernières et al., 1997). Rather, we accept the evidence supporting these two observations, and explore the thermal and rheological consequences of asthenospherization.

The upward migration of melt can be treated by a porous flow model analogous to that used for magma ascent under midoceanic ridges (Turcotte and Schubert, 2002). Assuming the solid matrix to be deformable in response to melt migration (a condition that should be favoured by an extensional environment) and a porosity with cubical symmetry (flow channels located along edges of cubes), the mean upward velocity of melt with respect to the matrix, driven by the vertical pressure gradient related to the density difference between melt and matrix, is:

$$\nu_{\mathrm{F}} = \frac{\psi d^2(\rho_{\mathrm{S}} - \rho_{\mathrm{F}})g}{24\pi\eta_{\mathrm{F}}} \tag{1}$$

and the mean flow per unit area (Darcy velocity) is:

$$\nu_{\mathrm{D}} = \frac{\nu_{\mathrm{F}}\psi}{3} \tag{2}$$

where ψ is the porosity, d the mean grain size, ρ_{S} and ρ_{F} matrix and melt densities, η_{F} the melt viscosity, and g is the acceleration of gravity. Taking, as orders of magnitude, $\psi = 0.01$, $d = 1$ mm, $\eta_{\mathrm{F}} = 10$ Pa s, and $\rho_{\mathrm{S}} - \rho_{\mathrm{F}} = 500\,\mathrm{kg\,m^{-3}}$, one has $\nu_{\mathrm{F}} \approx 2.0\,\mathrm{m\,a^{-1}}$, $\nu_{\mathrm{D}} \approx 6.7 \times 10^{-3}\,\mathrm{m\,a^{-1}}$. Realistic variations in porosity, grain size, and melt viscosity are unlikely to change these values by more than ± 1 order of magnitude. Consequently, percolation and impregnation of a 40 km thick section of lithospheric mantle would take approximately 20 ka $\pm$ 1 order of magnitude (provided, of course, that there is a continuous supply of melt and that the melt does not crystallize while ascending until the supply lasts). Although observational time constraints on peridotite impregnation are still lacking, these first-order considerations suggest that it should be a geologically fast process, with an upper limit characteristic time of 1 Ma at most, and much less if impregnation affects smaller thicknesses. The required total production of melt in the asthenosphere does not exceed a few percent by volume, if the volume from which melt is extracted is of the same order as the impregnated volume.

If the temperatures in the melt and the matrix are roughly the same (as shown by geothermometry), an analytical solution for one-dimensional advection of heat in a porous medium (Turcotte and Schubert, 2002) can be used to obtain a rough estimate of temperature in the ALM. The temperature distribution is given by:

$$T(z) = T_{\mathrm{a}} - (T_{\mathrm{a}} - T_0)\exp\left(\frac{\rho_{\mathrm{F}} c_{\mathrm{F}} \nu_{\mathrm{D}} z}{K_{\mathrm{S}}}\right) \tag{3}$$

where z is the depth measured from the top of the affected volume, T_{a} and T_0 are temperature at the bottom (asthenosphere) and top of the volume, ν_{D} the Darcy velocity, ρ_{F} and c_{F} are density and specific heat of the melt, and K_{S} is the thermal conductivity of the matrix (note that the exponent is negative because the velocity is upwards). Taking $\rho_{\mathrm{F}} = 2.8 \times 10^3\,\mathrm{kg\,m^{-3}}$, $c_{\mathrm{F}} = 1.0\,\mathrm{kJ\,kg^{-1}\,{}^{\circ}C^{-1}}$, $K_{\mathrm{S}} = 3.0\,\mathrm{W\,m^{-1}\,{}^{\circ}C^{-1}}$, ν_{D} as obtained from Eq. (2), $T_{\mathrm{a}} = 1250\,{}^{\circ}\mathrm{C}$, and the temperature gradient in the lithospheric mantle before heating as $10\,{}^{\circ}\mathrm{C\,km^{-1}}$, it can be seen from Eq. (3) that the temperature in the ALM is in the range $0.9T_{\mathrm{a}} \le T \le T_{\mathrm{a}}$ at all depths except in the top 10–15% of the impregnated zone. This result is independent of the thickness of the zone.

2.2. *Thermal model*

When taken together with observational evidence, the considerations developed in the previous subsection strongly suggest that the thermomechanical erosion of the lithosphere occurred – while the latter was being extended by plate boundary forces – in a geologically short time, and was accompanied by heating of the ALM to near-asthenospheric temperatures. Since the characteristic time of lithospheric extension is much longer than the characteristic time of impregnation, we assume as a first-order approximation than the heating was instantaneous.

Since neither the amount of stretching at the time of impregnation nor the thickness of the impregnated volume are known with any certainty, we parameterize the process in terms of an extension factor β and a lithosphere/melt interaction factor γ, the latter being the ratio between thickness of percolated volume and thickness of extended lithospheric mantle (Fig. 2). The choice of a uniform extension factor implicitly assumes that lithospheric thinning at the very large scale is achieved by bulk pure shear, which is not necessarily the case when the tectonic history is analyzed in detail (cf. e.g., Piccardo, 2003). However, the model is intended to estimate the one-dimensional thermorheological evolution in correspondence of the ALM, and should therefore retain its first-order validity.

The post-percolation thermal relaxation of the lithosphere is obtained from the one-dimensional heat conduction equation:

$$K\left(\frac{\partial^2 T}{\partial z^2}\right) = \rho c\left(\frac{\partial T}{\partial t}\right) - F \tag{4}$$

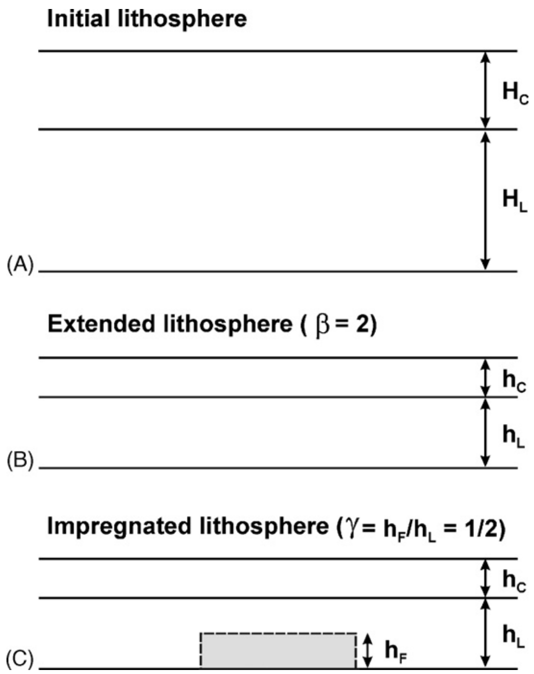

Fig. 2. Model geometry. (A) H_C and H_L are the initial thicknesses of crust and lithospheric mantle; (B) h_C and h_L are the corresponding thickness after extension; (C) h_F is the thickness of asthenospherized lithospheric mantle. The case for $\beta = 2$ and $\gamma = 1/2$ is shown.

where $T(z, t)$ is the temperature as function of depth z and time t, K the thermal conductivity, ρ the density, c the specific heat, and F is the heat production rate per unit volume. Table 1 shows the thermal and rheological model parameters used in the calculations. Properties are taken as constant in each layer. It is assumed that the volume affected by impregnation has temperature $T = T_a$ at $t = 0$; afterwards, it loses heat to the surrounding rocks. Eq. (4) is solved with the finite-difference code SHEMAT (cf. e.g., Clauser, 2003).

Figs. 3 and 4 show vertical temperature profiles in the lithosphere in correspondence of the centre of the ALM, as a function of thickness of impregnated volume at $t = 250$ ka after the beginning of cooling (Fig. 3) and as a function of time if the whole lithospheric mantle is affected (Fig. 4). In both cases, it is assumed that the lithosphere was extended by a factor $\beta = 2$ at the time of melt/lithospheric mantle interaction (thickness at the time of impregnation 60 km, of which the top 20 km consist of crust).

It can be seen from Fig. 3 that, within a short time after percolation, the ALM has begun to cool noticeably, while the lithosphere above is warming up. The lower crust is strongly affected if the percolation reaches levels close to the Moho ($\gamma \to 1$). This lower crustal temperature increase may cause local partial melting, especially for felsic compositions if volatiles are present.

Table 1
Thermal and rheological model parameters

Layer	Lithology	Thermophysical properties				Creep parameters		
		Thermal conductivity ($W\,m^{-1}\,K^{-1}$)	Thermal capacity ($MJ\,m^{-3}\,K^{-1}$)	Heat production ($\mu W\,m^{-3}$)	Density ($kg\,m^{-3}$)	A ($MPa^{-n}\,s^{-1}$)	n	E ($kJ\,mol^{-1}$)
Upper crust	Quartzite (wet)	2.5	2.5	1.4	2650	3.20×10^{-4}	2.3	154
Lower crust	Felsic granulite	2.1	2.5	0.4	2750	8.00×10^{-3}	3.1	243
Lower crust	Mafic granulite	2.1	2.5	0.4	2850	1.40×10^{4}	4.2	445
Lithospheric mantle	Dry peridotite	3.0	2.6	0.006	3300	2.50×10^{4}	3.5	532

Thermophysical parameters are used in Eq. (4); creep parameters in Eq. (7).

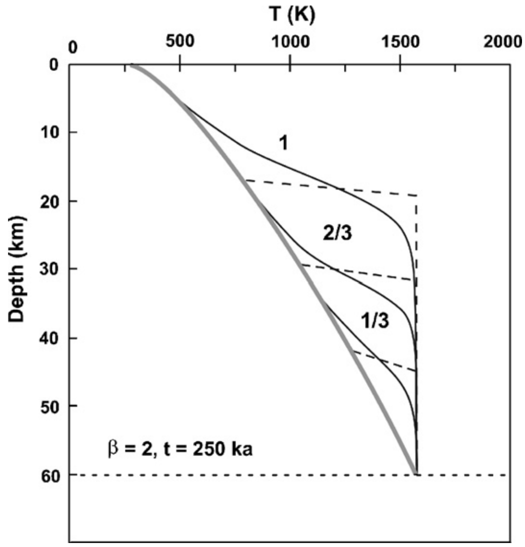

Fig. 3. Temperature distribution in the lithosphere along a vertical profile at the centre of the region affected by thermomechanical erosion as a function of thickness of ALM. The lithosphere has been extended by a factor $\beta = 2$ before asthenospherization (thickness 60 km). Thick grey line gives the temperature in the absence of heating; dashed and continuous lines give the initial temperature and the temperature 250 ka after heating (assumed instantaneous and followed by thermal relaxation) for three different γ values.

The time evolution of temperature shown in Fig. 4 demonstrates that thermal equilibrium is asymptotically reached ~10–20 Ma after the beginning of relaxation (note, however, that the attainment of equilibrium is a function of the depth of the initial thermal anomaly). There is, therefore, a relatively short time window in which the temperature distribution, and consequently the rheology, results in a maximum decrease in lithospheric strength. We examine the rheological consequences of the thermal evolution in the following subsection.

2.3. Rheological model

As is well known (cf. e.g., Ranalli, 1995), a first-order approximation of the rheology of the lithosphere as a function of depth is given by rheological profiles (strength envelopes). Although rheological profiles are subject to

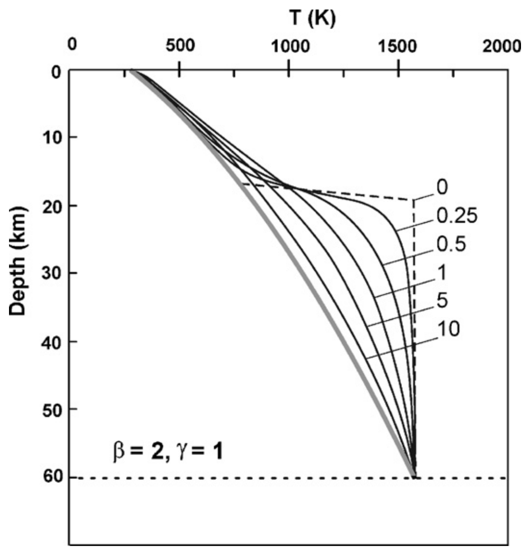

Fig. 4. Variations of temperature with time since asthenospherization for $\beta = 2$ and $\gamma = 1$. Numbers on continuous lines represent time (Ma) after instantaneous heating.

many uncertainties and assumptions (cf. the discussions in Ranalli, 1997; Fernández and Ranalli, 1997; Afonso and Ranalli, 2004), they are a reliable if approximate tool in order-of-magnitude estimates of the mechanical properties of the lithosphere.

Rheological profiles are constructed by comparing brittle frictional (Coulomb type) failure, high-pressure (plastic) failure, and power-law creep (viscous) behaviour, governed respectively by the equations (cf. Ranalli, 1995 for details):

$$\sigma_B \equiv \sigma_1 - \sigma_3 = \alpha\rho g z(1-\lambda) \tag{5}$$

$$\sigma_P \equiv \sigma_1 - \sigma_3 = \sigma_{crit} \tag{6}$$

$$\sigma_D \equiv \sigma_1 - \sigma_3 = \left(\frac{\varepsilon}{A}\right)^{1/n} \exp\left(\frac{E}{nRT}\right) \tag{7}$$

where σ_B, σ_P, and σ_D are the critical principal stress differences for frictional faulting, plastic faulting, and ductile creep, respectively. In Eq. (5), α is a parameter depending on frictional properties and type of faulting ($\alpha = 0.75$ for extensional faults with typical friction coefficient ~0.75), ρ the average density of rocks above depth z, and λ is the pore fluid factor (ratio of pore fluid pressure to lithostatic pressure in the rock, here taken to be hydrostatic, i.e., $\lambda = 0.4$). In Eq. (6), the critical (von Mises) stress is taken to be $\sigma_{crit} = 200$ MPa (Shimada, 1993; Renshaw and Schulson, 2004). In Eq. (7), ε is the strain rate (here assumed to be $10^{-14}\ s^{-1}$), A, n, and E are experimentally determined creep parameters and R is the gas constant (T in degrees Kelvin).

The frictional strength is linearly dependent on pressure (depth) but independent of temperature; the plastic strength is independent of pressure and shows only a weak dependence on temperature (here neglected); the creep strength is a strong function of temperature and its dependence on pressure can be neglected at lithospheric depths. The strength of the lithosphere at any depth is given by:

$$\sigma(z) = \mathrm{Min}\,\{\sigma_B, \sigma_P, \sigma_D\} \tag{8}$$

The total lithospheric strength (TLS) for a given rheological profile is obtained by integration of Eq. (8) over the thickness of the lithosphere H:

$$S = \int_H \sigma(z)\,dz \tag{9}$$

As a preliminary step, we estimate the rheology and TLS of an initially 120 km thick lithosphere (40 km of which consist of crust) subject to various amounts of extension ($1.0 \le \beta \le 2.5$), without any thermomechanical erosion. We assume the upper crust (initially 20 km thick) to have a rheology controlled by wet quartz. This is a common assumption, but in any case different rheologies would not have a significant effect, as the upper crust has for the most part frictional behaviour. Two different rheologies are considered for the lower crust (also 20 km thick): felsic and mafic granulite. The lithospheric mantle is assumed to have the rheology of dry peridotite. The creep parameters for these rock types are shown in Table 1.

Results, in terms of position and thickness of ductile layers, total strength of the individual components (upper crust, lower crust, lithospheric mantle), total lithospheric strength, and strength ratio (ratio of total strength for a given extension to total strength of unextended lithosphere) are given in Table 2. TLS values range from 5 to $10 \times 10^{12}\ N\,m^{-1}$ for unextended lithosphere to $2\text{–}3 \times 10^{12}\ N\,m^{-1}$ for $\beta = 2.5$. A mafic lower crust results in a TLS higher than that of a felsic lower crust by a factor decreasing from ~1.8 to ~1.3 with increasing extension. The strength ratio, after an initial small increase at low β due to the relatively larger effect of the reduction in thickness of the radioactive crust compared to adiabatic lithospheric thinning, decreases considerably; for $\beta = 2$, it is in the range of 0.5–0.7 for mafic and felsic lower crust, respectively. This softening effect of extension is well known (cf. e.g., Afonso and Ranalli, 2004). It is included here to emphasize that, in the case of Alpine peridotites, where thermomechanical erosion affected a lithosphere which was already thinned to about half its original thickness, the thinned TLS was 50–70% of the initial TLS.

We then explore the effects of lithosphere/melt interaction. The ALM is assumed to have the same creep behaviour as the lithospheric mantle, which implies that we model only the rheological changes caused by a change in temperature. The effect of a small volume fraction of melt on the rheology is likely to become important only above a critical melt threshold, whose value is subject to debate (cf. e.g., Vigneresse and Burg, 2004; Xu et al., 2004). While the melt

Table 2
Ductile depth ranges and lithospheric strengths as functions of extension factor β for different lower crustal rheologies

β	Upper crust		Lower crust				Lithospheric mantle		S_C		S_L		$S_\beta/S_{\beta 0}$	
	Ductile depth (km)	S_{UC} (N m^{-1})	Felsic granulite		Mafic granulite		Ductile depth (km)	S_{LM} (N m^{-1})	Felsic granulite (N m^{-1})	Mafic granulite (N m^{-1})	Felsic granulite (N m^{-1})	Mafic granulite (N m^{-1})	Felsic granulite	Mafic granulite
			Ductile depth (km)	S_{LC} (N m^{-1})	Ductile depth (km)	S_{LC} (N m^{-1})								
1	9.6–20	7.55×10^{11}	20–40	3.72×10^{11}	29.8–40	3.85×10^{12}	50–120	3.37×10^{12}	1.13×10^{12}	4.6×10^{12}	4.50×10^{12}	7.98×10^{12}	1	1
1.25	9.5–17.5	7.28×10^{11}	17.8–35	6.15×10^{11}	28–35	3.66×10^{12}	45.8–105	3.73×10^{12}	1.34×10^{12}	4.39×10^{12}	5.08×10^{12}	8.13×10^{12}	1.13	1.01
1.5	9.5–15	6.69×10^{11}	16.2–30	6.94×10^{11}	25–30	3.03×10^{12}	40–90	3.03×10^{12}	1.36×10^{12}	3.7×10^{12}	4.39×10^{12}	6.73×10^{12}	0.98	0.84
1.75	8.6–12.5	5.57×10^{11}	14.6–25	6.93×10^{11}	20–25	2.66×10^{12}	34.6–75	2.74×10^{12}	1.25×10^{12}	3.22×10^{12}	3.99×10^{12}	5.96×10^{12}	0.89	0.75
2	7.4–10	4.06×10^{11}	12.4–20	5.65×10^{11}	18–20	1.70×10^{12}	28.4–60	2.32×10^{12}	9.71×10^{11}	2.1×10^{12}	3.29×10^{12}	4.42×10^{12}	0.73	0.55
2.25	7.2–8.9	3.65×10^{11}	11.2–17.8	4.71×10^{11}	16.6–17.8	1.41×10^{12}	25–53	2.01×10^{12}	8.36×10^{11}	1.78×10^{12}	2.84×10^{12}	3.78×10^{12}	0.63	0.47
2.5	6.2–8	2.76×10^{11}	10.2–16	4.01×10^{11}	14.9–16	1.14×10^{12}	22.6–48	1.83×10^{12}	6.77×10^{11}	1.41×10^{12}	2.50×10^{12}	3.24×10^{12}	0.56	0.40

S denotes the total strength of a given layer; the subscripts UC, LC, C, LM, and L refer to upper crust, lower crust, total crust, lithospheric mantle, and total lithosphere, respectively; $S_\beta/S_{\beta 0}$ is the ratio between lithospheric strength for a given extension factor and lithospheric strength before extension.

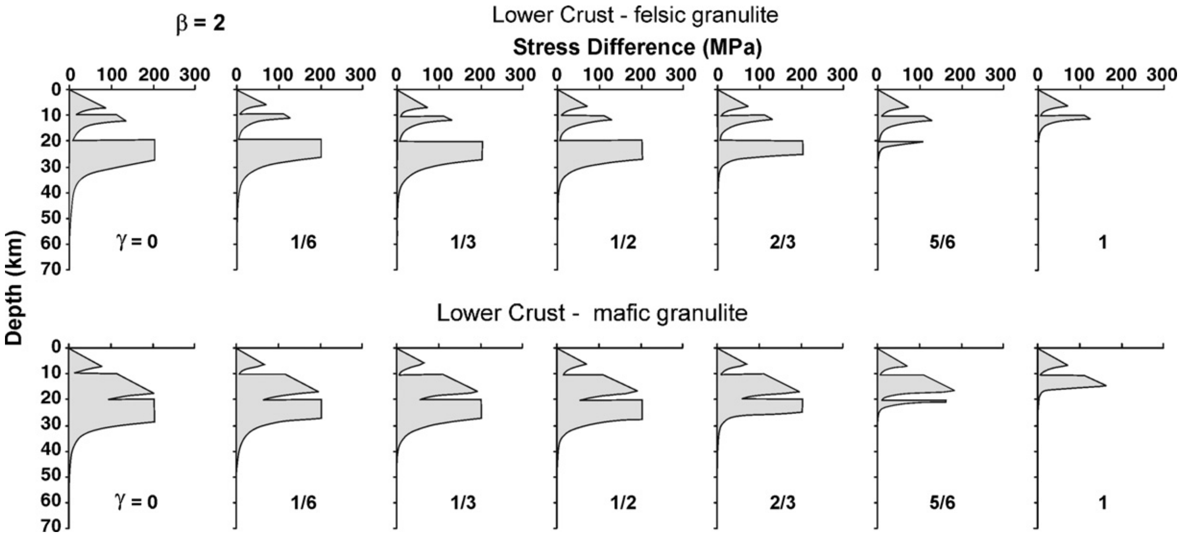

Fig. 5. Rheological profiles at $t = 250$ ka after heating for extension factor $\beta = 2$, various thicknesses of ALM, and two lower crustal rheologies.

fraction may be an important factor in localizing the deformation, its effect on the bulk rheology of the ALM should be marginal in comparison with the thermal effect, which by itself reduces the creep strength to very small values.

The rheological profiles for an extended ($\beta = 2$) lithosphere at $t = 250$ ka after impregnation are shown in Fig. 5 for various γ values and two lower crustal compositions (felsic and mafic). The temperature profiles shown in Fig. 3 have been used in the calculations. As the relative thickness of the ALM increases, the rheological effect of the temperature increase becomes more significant, as harder and harder parts of the lithospheric mantle become asthenospherized. As $\gamma \to 1$ (the percolation approaches the Moho), the thermomechanical erosion affects also the lower crust, as a consequence of its temperature increase. This is particularly evident in the case of mafic composition.

The rheological effects of asthenospherization are shown in Table 3 as a function of thickness of ALM for $\beta = 2$, $t = 250$ ka; variations in TLS are given in Figs. 6 and 7. It can be seen that the effect of asthenospherization is highly non-linear. The reason for this, as explained above, is that the strength contrast between lithospheric mantle and ALM becomes larger for higher initial creep strengths (see Fig. 5). If thermomechanical erosion affects only the lower parts of the lithospheric mantle (say, for $\gamma < 0.5$), the reduction in TLS is less than 20%. For larger γ values, however, the effect increases rapidly, leading to TLS reductions of the order of 80% if the ALM reaches up to the Moho.

Since asthenospherization by lithosphere/melt interaction is a fast process, the softening of the ALM has been assumed instantaneous above, and a snapshot given of the situation at a given time after the beginning of thermal relaxation. The variations of the rheological properties as a function of time are given in Table 4 for the limiting

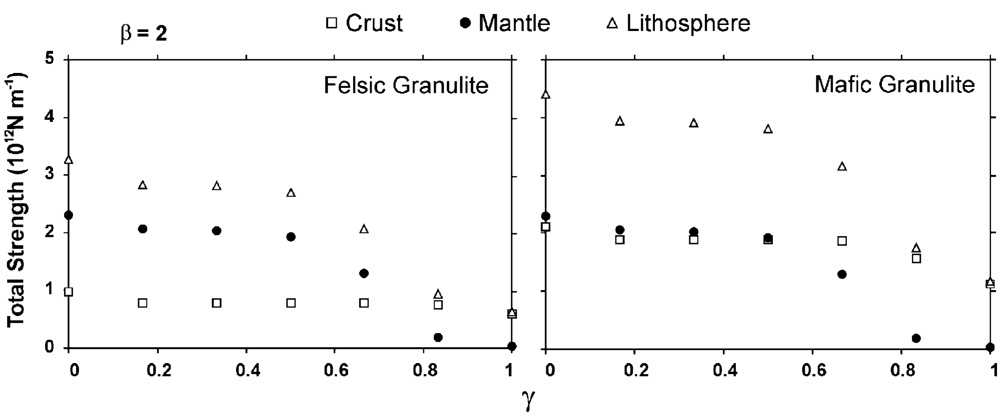

Fig. 6. Strengths of crust, lithospheric mantle and total lithosphere at $t = 250$ ka after heating for $\beta = 2$ and varying thickness of ALM.

Table 3
Effect of volume of impregnated zone on rheology and lithospheric strength for $\beta = 2$

γ	Upper crust		Lower crust				Lithospheric mantle		S_C		S_L		$S_\gamma/S_{\gamma 0}$	
	Ductile depth (km)	S_{UC} (N m^{-1})	Felsic granulite		Mafic granulite		Ductile depth (km)	S_{LM} (N m^{-1})	Felsic granulite (N m^{-1})	Mafic granulite (N m^{-1})	Felsic granulite (N m^{-1})	Mafic granulite (N m^{-1})	Felsic granulite	Mafic granulite
			Ductile depth (km)	S_{LC} (N m^{-1})	Ductile depth (km)	S_{LC} (N m^{-1})								
0	7.4–10	4.06×10^{11}	12.4–20	5.7×10^{11}	18–20	1.7×10^{12}	28.4–60	2.3×10^{12}	9.76×10^{11}	2.1×10^{12}	3.29×10^{12}	4.42×10^{12}	1	1
1/6	6.7–10	3.38×10^{11}	11.6–20	4.43×10^{11}	17.1–20	1.55×10^{12}	27.5–60	2.06×10^{12}	7.81×10^{11}	1.88×10^{12}	2.84×10^{12}	4.04×10^{12}	0.86	0.91
1/3	6.7–10	3.38×10^{11}	11.6–20	4.43×10^{11}	17.1–20	1.55×10^{12}	27–60	2.03×10^{12}	7.81×10^{11}	1.88×10^{12}	2.81×10^{12}	3.9×10^{12}	0.85	0.88
1/2	6.7–10	3.38×10^{11}	11.6–20	4.43×10^{11}	17.1–20	1.55×10^{12}	26.9–60	1.92×10^{12}	7.81×10^{11}	1.88×10^{12}	2.7×10^{12}	3.8×10^{12}	0.82	0.86
2/3	6.7–10	3.38×10^{11}	11.6–20	4.42×10^{11}	17.1–20	1.53×10^{12}	24.8–60	1.29×10^{12}	7.80×10^{11}	1.87×10^{12}	2.07×10^{12}	2.9×10^{12}	0.63	0.66
5/6	6.7–10	3.38×10^{11}	11.6–20	4.08×10^{11}	16.1–20	1.23×10^{12}	20.1–60	1.92×10^{11}	7.46×10^{11}	1.56×10^{12}	9.46×10^{11}	1.75×10^{12}	0.29	0.40
1	6.7–10	3.32×10^{11}	11.1–20	2.57×10^{11}	14.3–20	7.93×10^{11}	20.1–60	4.15×10^{10}	5.89×10^{11}	1.12×10^{12}	6.32×10^{11}	1.17×10^{12}	0.19	0.26

Symbols as in Table 2; $S_\gamma/S_{\gamma 0}$ is the ratio between lithospheric strength for a given thickness of ALM and strength without asthenospherization.

Table 4
Time variations of lithospheric strength after impregnation for $\beta = 2$ and $\gamma = 1$

Time (Ma)	Upper crust		Lower crust				Lithospheric mantle		S_C		S_L		S_t/S_{t0}	
			Felsic granulite		Mafic granulite									
	Ductile depth (km)	S_{UC} (N m^{-1})	Ductile depth (km)	S_{LC} (N m^{-1})	Ductile depth (km)	S_{LC} (N m^{-1})	Ductile depth (km)	S_{LM} (N m^{-1})	Felsic granulite (N m^{-1})	Mafic granulite (N m^{-1})	Felsic granulite (N m^{-1})	Mafic granulite (N m^{-1})	Felsic granulite	Mafic granulite
0	7.4–10	4.06×10^{11}	12.4–20	5.7×10^{11}	18–20	1.7×10^{12}	28.4–60	2.3×10^{12}	9.72×10^{11}	2.1×10^{12}	3.29×10^{12}	4.42×10^{12}	1	1
0.01	6.7–10	3.34×10^{11}	11.6–20	4.14×10^{11}	17.1–20	1.24×10^{12}	20–60	1.29×10^{10}	48×10^{11}	1.57×10^{12}	7.61×10^{11}	1.59×10^{12}	0.23	0.36
0.25	6.7–10	3.34×10^{11}	11.2–20	2.57×10^{11}	14.3–20	7.93×10^{11}	20.1–60	4.15×10^{10}	5.91×10^{11}	1.12×10^{12}	6.32×10^{11}	1.17×10^{12}	0.19	0.26
0.5	6.4–10	2.97×10^{11}	10.1–20	1.21×10^{11}	13.1–20	6×10^{11}	20.4–60	1.04×10^{11}	4.19×10^{11}	8.97×10^{11}	5.23×10^{11}	1.0×10^{12}	0.16	0.23
1	5.5–10	2.33×10^{11}	10.1–20	6.23×10^{10}	12.5–20	5.1×10^{11}	20.4–60	1.20×10^{11}	2.95×10^{11}	7.44×10^{11}	4.15×10^{11}	8.64×10^{11}	0.13	0.19
5	5.8–10	2.57×10^{11}	10.04–20	1.45×10^{11}	14.2–20	8.9×10^{11}	20–60	6.59×10^{11}	4.03×10^{11}	1.15×10^{12}	1.06×10^{12}	1.81×10^{12}	0.32	0.41
10	6.9–10	3.54×10^{11}	11.58–20	4.08×10^{11}	16.4–20	1.4×10^{12}	25.2–60	1.64×10^{12}	7.62×10^{11}	1.73×10^{12}	2.40×10^{12}	3.43×10^{12}	0.73	0.77
20	7.4–10	3.96×10^{11}	12.22–20	5.26×10^{11}	17.4–20	1.6×10^{12}	26.9–60	2.04×10^{12}	9.23×10^{11}	1.97×10^{12}	2.96×10^{12}	4.01×10^{12}	0.90	0.91

Symbols as in Tables 2 and 3; S_t/S_{t0} is the ratio between lithospheric strength at a given time after asthenospherization and strength in the absence of thermomechanical erosion.

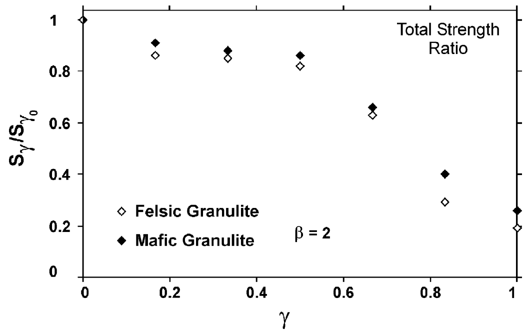

Fig. 7. Total lithospheric strength ratio (see also Table 3) at $t = 250$ ka for $\beta = 2$ and various ALM thicknesses.

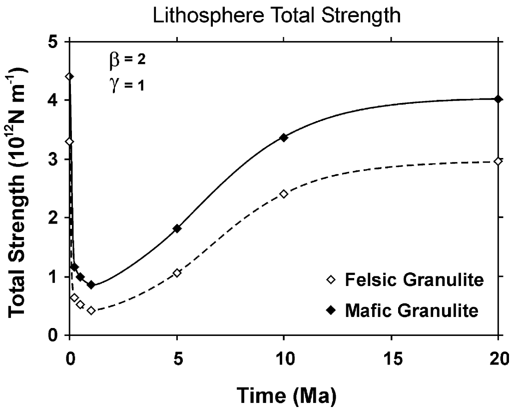

Fig. 8. Variations of TLS with time since impregnation for $\beta = 2$, $\gamma = 1$, and two lower crustal rheologies.

case $\gamma = 1$; TLS variations are given in Figs. 8 and 9. The maximum softening effect is reached within ∼1–2 Ma from asthenospherization, when TLS is reduced to 0.1–0.2 of its initial value. This represent a small (∼6%) further decrease from the situation at $t = 0.25$ Ma, and is very likely to be within the margins of error stemming from thermal approximations and rheological assumptions. However, the strong reduction in TLS is a transient episode. Neglecting decreases caused by further thinning, the TLS has recovered to 75% of its initial value 10 Ma after asthenospherization, and to 90% after 20 Ma (the times depend on the amount of thinning before asthenospherization, and are shorter for larger amounts of extension). There is, therefore, a time window when the lithosphere is at its softest, and consequently most susceptible to whole lithospheric failure and initiation of sea-floor spreading.

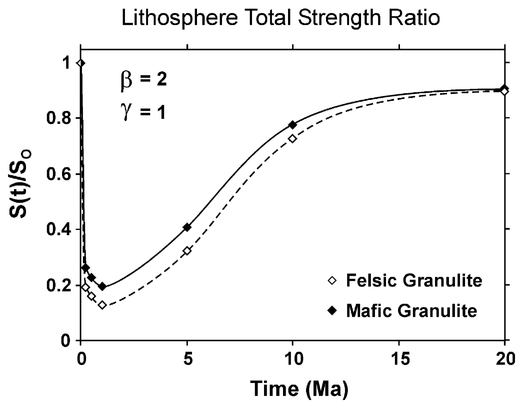

Fig. 9. Time variations of strength ratio (see also Table 4) for the same conditions shown in Fig. 8.

3. Conclusions

Percolation and impregnation of the overlying lithosphere by upwardly migrating asthenospheric melts, accompanied by a concomitant increase in temperature, is strongly supported by observation. Field evidence shows that affected thicknesses of lithospheric mantle must have been considerable.

Migration of melt fractions from the asthenosphere to the overlying mantle lithosphere can result in the thermomechanical erosion of the lithosphere. Although other factors can play a role during extension (e.g., crustal underplating, polyphase thermal history; cf. e.g., Pasquale et al., 2003; Verdoya et al., 2005), we have focused on asthenospherization as our basic working hypothesis, and have estimated its rheological consequences under simplified but reasonable assumptions.

The basic idea underlying the model presented in this paper is that the transition from continental extension to oceanic spreading (that is, the onset of whole lithospheric failure, whereby one plate is separated into two plates) must occur where the TLS is considerably reduced. Plate tectonic forces are of the order of 10^{12}–10^{13} N m^{-1} (cf. Turcotte and Schubert, 2002), that is, of the same order of magnitude as the TLS of continental lithosphere (Ranalli, 1991, 1995; Afonso and Ranalli, 2004). The most obvious process for reducing the TLS is thermal softening, and the most obvious agents are mantle plumes (cf. e.g., Schubert et al., 2001). Heat diffusion from sublithospheric plume heads, however, has a characteristic time >10 Ma for lithospheric thickness >20 km, and much longer for thicker lithosphere. As an agent for softening the continental lithosphere, therefore, plumes are effective only in time frames of the order of tens of millions of years.

If the possibility of fast asthenospherization is admitted, the rheological consequences are relevant to the problem of initiation of oceanic spreading in an extending continental lithosphere. Nothing much happens if the thickness of the ALM is only a minor part of the thickness of the lithospheric mantle. If however, the affected thickness is large and the melt fraction approaches the Moho, the TLS can be reduced to 10–50% of the initial strength (of the extended lithosphere). Moreover, the maximum reduction in TLS is achieved within a short time span ($\sim$1 Ma as an order of magnitude) after asthenospherization.

Therefore, the possibility exists that the thermomechanical erosion of the lithosphere, as described in this paper, could be a contributing or controlling factor in the rapid transition from continental extension to whole lithospheric failure and sea-floor spreading.

Acknowledgements

G. Ranalli's work is financially supported by a grant from NSERC (Natural Sciences and Engineering Research Council of Canada). G.B. Piccardo's work is financially supported by the Italian MIUR—Ministero dell'Istruzione, Università e Ricerca (PRIN2005: "Lithosphere evolution induced by migration of mantle-derived melts in different geodynamic settings"), the University of Genova, and the Italian Consiglio Nazionale delle Ricerche (CNR). P. Corona-Chávez took part in this work while on sabbatical at Carleton University, Ottawa, Canada in 2003/2004. We thank Gianreto Manatschal and an anonymous reviewer for criticism and suggestions, which helped us to revise the paper, and Riccardo Polino for editorial help.

References

Afonso, J.C., Ranalli, G., 2004. Crustal and mantle strengths in continental lithosphere: is the jelly sandwich model obsolete? Tectonophysics 394, 221–232.

Beccaluva, L., Piccardo, G.B., 1978. Petrology of the northern Apennine ophiolites and their significance in the Western Mediterranean area. In: Closs, H., Roeder, D., Schmidt, K. (Eds.), Alps, Apennines, Hellenides. Inter-Union Commission on Geodynamics, pp. 243–254 (Rep. 38).

Clauser, C. (Ed.), 2003. Numerical Simulation of Reactive Flow in Hot Aquifers. Springer, Berlin.

Decandia, F.A., Elter, P., 1972. La "zona" ofiolitifera del Bracco nel settore compreso fra Levanto e la Val Graveglia (Appennino Ligure). Mem. Soc. Geol. Ital. 11, 503–530.

Dewey, J.F., Pittman, W.C., Ryan, W.B.F., Bonnin, J., 1973. Plate tectonics and the evolution of the Alpine system. Geol. Soc. Am. Bull. 84, 3137–3180.

Drury, M.R., Strating, E.H.H., Vissers, R.L.M., 1990. Shear zone structures and microstructures in mantle peridotites from the Voltri Massif, Ligurian Alps, NW Italy. Geol. Mijnb. 69, 3–17.

Fernández, M., Ranalli, G., 1997. The role of rheology in extensional basin formation modelling. Tectonophysics 282, 129–145.
Lemoine, M., Tricart, P., Boillot, G., 1987. Ultramafic and gabbroic ocean floor of the Ligurian Tethys (Alps, Corsica, Apennines): in search of a genetic model. Geology 15, 622–625.
McKenzie, D., 1985. The extraction of magma from the crust and mantle. Earth Planet. Sci. Lett. 74, 81–91.
McKenzie, D., 1989. Some remarks on the movement of small melt fractions in the mantle. Earth Planet. Sci. Lett. 95, 53–72.
Muntener, O., Hermann, J., 1996. The Val Malenco lower crust-upper mantle complex and its field relations (Italian Alps). Schweizer. Mineral. Petrogr. Mitt. 76, 475–500.
Müntener, O., Piccardo, G.B., 2003. Melt migration in ophiolites: the message from Alpine–Apennine peridotites and implications for embryonic ocean basins. In: Dilek, Y., Robinson, P.T. (Eds.), Ophiolites in Earth History. Geol. Soc. Lond., pp. 69–89 (Sp. Publ. 218).
Müntener, O., Hermann, J., Trommsdorff, V., 2000. Cooling history and exhumation of lower crust and upper mantle (Malenco, eastern central Alps). J. Petrol. 41, 175–200.
Müntener, O., Piccardo, G.B., Polino, R., Zanetti, A., 2005. Mantle processes and geodynamic significance of the Lanzo peridotite (NW Italy): "asthenospherization" of ancient mantle lithosphere. Ofioliti 30, 113–126.
Pasquale, V., Verdoya, M., Chiozzi, P., 2003. Heat flux budget in the southeastern continental margin of the Tyrrhenian basin. Phys. Chem. Earth 28, 407–420.
Piccardo, G.B., 1976. Petrologia del massiccio lherzolitico di Suvero (La Spezia). Ofioliti 1, 279–317.
Piccardo, G.B., 1977. Le ofioliti dell'area ligure: petrologia e ambiente geodinamico di formazione. Rend. Soc. Ital. Miner. Petrol. 33, 221–252.
Piccardo, G.B., 2003. Mantle processes during ocean formation: petrologic records in peridotites from the Alpine–Apennine ophiolites. Episodes 26, 193–200.
Piccardo, G.B., Rampone, E., Vannucci, R., 1990. Upper mantle evolution during continental rifting and ocean formation: evidence from peridotite bodies of the Western Alpine-Northerrn Apennine system. Mem. Soc. Geol. France 156, 323–333.
Piccardo, G.B., Müntener, O., Zanetti, A., Pettke, T., 2004a. Ophiolitic peridotites of the Alpine–Apennine system: mantle processes and geodynamic relevance. Int. Geol. Rev. 46, 1119–1159.
Piccardo, G.B., Müntener, O., Zanetti, A., 2004b. Alpine–Apennine ophiolitic peridotites: new concepts on their composite evolution. Ofioliti 29, 63–74.
Piccardo, G.B., Zanetti, A., Spagnolo, G., Poggi, E., 2005. Recent researches on melt–rock interaction in the Lanzo South peridotite. Ofioliti 30, 137–162.
Piccardo, G.B., Zanetti, A., Poggi, E., Spagnolo, G., Müntener, O., in press. Melt/peridotite interaction in the southern Lanzo peridotite: field, textural and geochemical evidence. Lithos.
Piccardo, G.B., Poggi, E., Vissers, R.L.M., 2007. The pre-oceanic evolution of the Erro-Tobbio peridotite (Voltri Massif—Ligurian Alps, Italy). J. Geodyn. 43, 417–449.
Rampone, E., Piccardo, G.B., 2000. The ophiolite-oceanic lithosphere analogue: new insights from the Northern Apennines (Italy). In: Dilek, Y., Moores, E.M., Elthon, D., Nicolas, A. (Eds.), Ophiolites and Oceanic Crust: New Insights from Field Studies and the Ocean Drilling Program. Geol. Soc. America Sp. Paper 349, 21–34.
Rampone, E., Piccardo, G.B., Vannucci, R., Bottazzi, P., Ottolini, L., 1993. Subsolidus reactions monitored by trace element partitioning: the spinel-to plagioclase-facies transition in mantle peridotites. Contr. Miner. Petrol. 115, 1–17.
Rampone, E., Hofmann, A.W., Piccardo, G.B., Vannucci, R., Bottazzi, P., Ottolini, L., 1995. Petrology, mineral and isotope geochemistry of the External Ligurides peridotites (Northern Apennines, Italy). J. Petrol. 36, 81–105.
Rampone, E., Hofman, A.W., Raczek, I., 1998. Isotopic contrasts within the Internal Liguride ophiolite (N. Italy): the lack of a genetic mantle-crust link. Earth Planet. Sci. Lett. 163, 175–189.
Ranalli, G., 1991. Regional variations in lithosphere rheology from heat flow observations. In: Cermak, V., Rybach, L. (Eds.), Terrestrial Heat Flow and the Lithosphere Structure, vol. 1–22. Springer, Berlin.
Ranalli, G., 1995. Rheology of the Earth, 2nd ed. Chapman & Hall, London.
Ranalli, G., 1997. Rheology of the lithosphere in space and time. In: Burg, J.P., Ford, M. (Eds.), Orogeny through Time. Geol. Soc. Lond., pp. 19–37 (Sp. Publ. 121).
Renshaw, C.E., Schulson, E.M., 2004. Plastic faulting: brittle-like failure under high confinement. J. Geophys. Res. 109, doi:10.1029/2003JB002945.
Schubert, G., Turcotte, D.L., Olson, P., 2001. Mantle Convection in the Earth and Planets. University Press, Cambridge.
Seitz, H.M., Altherr, R., Ludwig, T., 1999. Partitioning of transition elements between orthopyroxene and clinopyroxene in peridotitic and websteritic xenoliths: new empirical geothermometers. Geochim. Cosmochim. Acta 63, 3967–3982.
Shimada, M., 1993. Lithosphere strength inferred from fracture strength of rocks at high confining pressures and temperatures. Tectonophysics 217, 55–64.
Strating, E.H.H., Rampone, E., Piccardo, G.B., Drury, M.R., Vissers, R.L.M., 1993. Subsolidus emplacement of mantle peridotites during incipient oceanic rifting and opening of the Mesozoic Tethys (Voltri Massif, NW Italy). J. Petrol. 34, 901–927.
Trommsdorff, V., Piccardo, G.B., Montrasio, A., 1993. From magmatism through metamorphism to sea-floor emplacement od subcontinental Adria lithosphere during pre-Alpine rifting (Malenco, Italy). Schweizer. Mineral. Petrogr. Mitt. 73, 191–203.
Turcotte, D.L., Schubert, G., 2002. Geodynamics, 2nd ed. University Press, Cambridge.
Verdoya, M., Pasquale, V., Chiozzi, P., 2005. Thermomechanical evolution and rheology of the northern sector of the tyrrhenian–Apennines system. J. Volcanol. Geotherm. Res. 148, 20–30.
Vernières, J., Godard, M., Bodinier, J.-L., 1997. A plate model for the simulation of trace element fractionation during partial melting and magma transport in the Earth's upper mantle. J. Geophys. Res. 102, 24771–24784.

Vigneresse, J.L., Burg, J.P., 2004. Strain-rate dependent rheology of partially molten rocks. In: Grocott, J., McCaffrey, K.J.W., Taylor, G., Tikoff, B. (Eds.), Vertical Coupling and Decoupling in the Lithosphere. Geol. Soc. Lond., pp. 327–336 (Sp. Publ. 227).

Vissers, R.L.M., Drury, M.R., Strating, E.H.H., van der Wal, D., 1991. Shear zones in the upper mantle: a case study in an Alpine lherzolite massif. Geology 19, 990–993.

Xu, Y., Zimmerman, M.E., Kohlstedt, D.L., 2004. Deformation behaviour of partially molten rocks. In: Karner, G.D., Taylor, B., Driscoll, N.W., Kohlstedt, D.L. (Eds.), Rheology and Deformation of the Lithosphere at Continental Margins. Columbia University Press, New York, pp. 284–310.